Materials Science and Engineering B 178 (2013) 630–634

Contents lists available at SciVerse ScienceDirect

Materials Science and Engineering B

journal homepage: www.elsevier.com/locate/mseb

Short communication

Plasmonic back contacts with non-ordered Ag nanostructures for light trapping in thin-film silicon solar cells

Ulrich W. Paetzold*, Matthias Meier[1], Etienne Moulin[2], Vladimir Smirnov[3], Bart E. Pieters[4], Uwe Rau[5], Reinhard Carius[6]

IEK5-Photovoltaik, Forschungszentrum Juelich, D-52425 Juelich, Germany

ARTICLE INFO

Article history:
Received 26 June 2012
Received in revised form
10 September 2012
Accepted 11 October 2012
Available online 25 October 2012

Keywords:
Thin-film solar cell
Light trapping
Plasmonic
Nanostructures

ABSTRACT

In this work, we investigate the light trapping of thin-film silicon solar cells which apply plasmonic Ag back contacts with non-ordered Ag nanostructures. The preparation, characterization and three-dimensional electromagnetic simulations of these back contacts with various distributions of non-ordered Ag nanostructures are presented. The measured reflectance spectra of the Ag back contacts with non-ordered nanostructures in air are well reproduced in reflectance spectra derived from the three-dimensional electromagnetic simulations of isolated nanostructures on Ag back contacts. The light–matter interaction of these nanostructures is given by localized surface plasmons and, thus, the measured diffuse reflectance of the back contacts is attributed to plasmon-induced light scattering. A significant plasmonic light-trapping effect in n-i-p substrate-type μc-Si:H thin-film solar cell prototypes which apply a Ag back contact with non-ordered nanostructures is identified when compared with flat reference solar cells.

1. Introduction

Thin-film silicon solar cells made of amorphous (a-Si:H) or microcrystalline silicon (μc-Si:H) require an advanced light trapping in order to efficiently absorb incident light of wavelengths longer than 500 nm [1–3]. In this spectral range, the a-Si:H and μc-Si:H absorber layers are optically thin. State-of-the-art thin-film silicon solar cells apply randomly textured interfaces at the front and rear side to scatter and diffract incident light into the device [3,4]. This scattered light is partly guided in the silicon absorber layers which leads to an enhanced short-circuit current density (J_{sc}) of the solar cell.

To further improve the light trapping in thin-film silicon solar cells several, new concepts are studied in the literature. One of these concepts applies light-scattering plasmonic nanostructures [5–8]. At metal nanoparticles or nanostructured metal layers, light can couple efficiently to localized surface plasmon (LSP) [9]. A dominant radiative decay of the LSP resonances induces very efficient scattering of incident light. If this LSP-induced light scattering is directed into the absorber layer of a thin-film silicon solar cell, the metal nanostructures serve as sub-wavelength scattering components that couple incident propagating light into the thin absorber layers of the solar cells. Based on this approach, metal nanostructures placed at the front interface of solar cells have been proposed to reduce the initial reflection of the solar cell as well as increasing the light path in the absorber layer [10,11]. At the rear side of the solar cell, periodic and non-ordered Ag nanoparticles and Ag nanostructures have been applied to scatter incident light such that the light is guided in the absorber layers of the solar cell [12–17].

Recently, we showed by means of electromagnetic simulations that nanostructures on Ag back contacts of μc-Si:H solar cells exhibit particularly promising light-scattering properties for light-trapping [18]. In the present study, such non-ordered nanostructures on the Ag back contact of μc-Si:H thin-film solar cells were experimentally realized. The measured diffuse reflectance spectra of these back contacts are compared to the simulated diffuse reflectance spectra. This allows for a straightforward analysis of the contribution of the plasmon-induced light scattering to the diffuse reflectance spectra of the Ag back contacts with non-ordered Ag nanostructures.

* Corresponding author. Tel.: +49 2461 61 8987.
E-mail addresses: u.paetzold@fz-juelich.de (U.W. Paetzold), ma.meier@fz-juelich.de (M. Meier), e.moulin@fz-juelich.de (E. Moulin), v.smirnov@fz-juelich.de (V. Smirnov), b.pieters@fz-juelich.de (B.E. Pieters), u.rau@fz-juelich.de (U. Rau), r.carius@fz-juelich.de (R. Carius).
[1] Tel.: +49 2461 61 1552.
[2] Tel.: +49 2461 61 2069.
[3] Tel.: +49 2461 61 4855.
[4] Tel.: +49 2461 61 2679.
[5] Tel.: +49 2461 61 1554.
[6] Tel.: +49 2461 61 4508.

0921-5107/$ – see front matter © 2012 Elsevier B.V. All rights reserved.
http://dx.doi.org/10.1016/j.mseb.2012.10.013

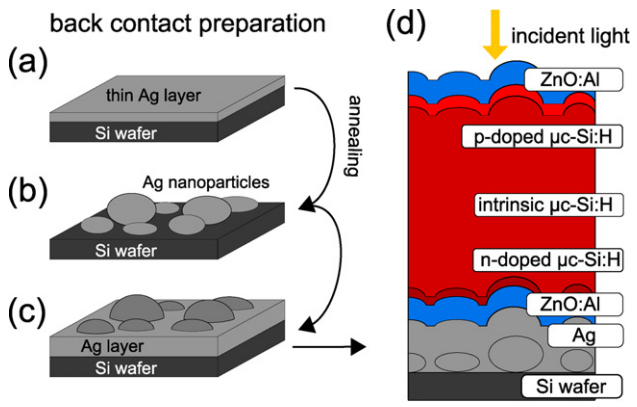

Fig. 1. (a)–(c) Schematic illustration of the preparation of the plasmonic Ag back contacts with non-ordered nanostructures. (d) Schematic cross-section of a n-i-p substrate-type µc-Si:H solar cell deposited on a plasmonic back contact with non-ordered Ag nanostructures.

2. Methods

2.1. Preparation of Ag back contact with non-ordered nanostructures

The fabrication steps from the Ag nanoparticles to the Ag back contacts with non-ordered nanostructures are schematically illustrated in Fig. 1(a)–(c). The Ag back contacts are prepared for the subsequent deposition of a n-i-p substrate-type µc-Si:H thin-film silicon solar cell (see Fig. 1(d)).

Non-ordered distributions of Ag nanoparticles on silicon wafer substrates were prepared by annealing thermally evaporated Ag films for 6 h at 500 °C in a nitrogen atmosphere (see Fig. 1(a) and (b)). During this annealing process, due to the surface tension of the Ag, the Ag films agglomerated into non-ordered distributions of Ag nanoparticles [12–15]. Scanning electron microscopy images of three Ag nanoparticle distributions are shown in Fig. 2. For these samples, the initial Ag film thickness varied from 10 nm to 30 nm. A clear correlation between the initial Ag film thickness and the average size of the Ag nanoparticles is apparent. Finally, the silicon wafer substrates with the Ag nanoparticle distributions were covered with a 200 nm thick dc-sputtered Ag (see Fig. 1(c)). The resulting surface of a Ag back contact exhibits half-ellipsoidal Ag nanostructures.

In this study five distinct types of distributions of Ag nanostructures are investigated which were prepared on nanoparticles obtained by annealing of Ag layers of thickness of 10 nm, 15 nm, 20 nm, 30 nm and 40 nm. These five back contacts are referred to as Type I–Type V. In order to analyze the nanostructure distribution, atomic force microscopy (AFM) images of the back contacts were analyzed with the Advanced Threshold Algorithm of the Particle and Pore Analysis module of the SPIP software [20]. The very sensitive detection level for the algorithm was set to the mean level of plane-fitted AFM data. Those nanostructures with a height to radius aspect ratio below 0.5 and a radius below 3 nm have been excluded. From the detected nanostructure distribution, the area-weighted base radius and the height of the nanostructures were derived.

The diffuse reflectance spectra of the Ag back contacts with non-ordered Ag nanostructures were measured with a spectrophotometer LAMBDA 950 (Perkin Elmer) equipped with an integrating Ulbricht sphere.

2.2. Electromagnetic simulations

The interaction of light with isolated plasmonic Ag nanostructures on the Ag back contact was studied with a three-dimensional numerical solver of Maxwell's equations. The simulations were carried out with the program JCMsuite® which applies the Finite Element Method to discretize Maxwell's equations on a on prismatic grid in all three dimensions [21]. Similar nanostructures than those studied in this work have been investigated in detail with the same method in [18]. From the simulated three-dimensional electric field distributions, power loss spectra as well as the diffuse and total reflectance spectra were calculated.

2.3. Solar cell preparation

We prepared µc-Si:H solar cells in n-i-p substrate configuration with an active cell area of 1 cm × 1 cm (see Fig. 1(d)). The performance of solar cells deposited on (i) a flat reference Ag back contact, (ii) conventional randomly textured Ag back contacts and (iii) a Ag back contact with non-ordered Ag nanostructures were compared. Back contact (iii) is prepared on a Type IV Ag back contacts with non-ordered nanostructures. The preparation is described in Section 2.1. The state-of-the-art random texture of the Ag back contact (ii) is prepared by wet-chemical etching of a rf-sputtered ZnO:Al substrate for 40 s in 0.5 w/w% HCl [3]. On top of all back contacts, a 80 nm (±5 nm) thick ZnO:Al layer was sputtered at room temperature by rf-sputtering. Afterwards, a n-doped, an intrinsic and a p-doped µc-Si:H layer were deposited by plasma enhanced chemical vapor deposition [19]. The thicknesses of these layers are 20 nm (±10 nm), 1100 nm (±25 nm) and 20 nm (±10 nm), respectively. For the front contact, a 70 nm (±10 nm) thick front ZnO:Al layer in combination with Ag finger electrodes was deposited. The external quantum efficiency (*EQE*) of the solar cells is used to evaluate the influence of the plasmonic Ag back contact with non-ordered Ag nanostructures on the light trapping of the solar cell in the relevant spectral region.

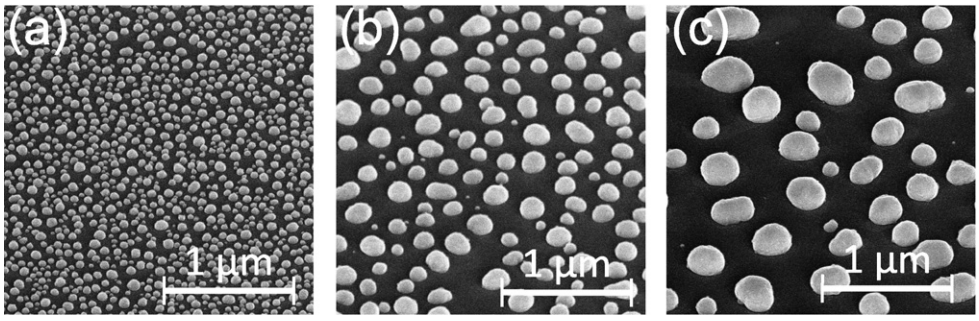

Fig. 2. Scanning electron microscopy images of Ag nanoparticles prepared by annealing of thin Ag films of thickness of 10 nm, 20 nm, and 30 nm from (a), (b), (c), respectively.

3. Results and discussion

3.1. Characterization of Ag back contact with non-ordered nanostructures

In Fig. 3(a)–(e), AFM images of the Ag back contact surface are shown for the five types of nanostructure distributions. Due to conformal deposition of the Ag layer onto the Ag nanoparticles, the five types of Ag back contacts reveal non-ordered nanostructures. In Fig. 3(f), the detected area-weighted base radius distributions of the five types of back contact are shown. It is seen that the average base radius of the nanostructures on the Ag back contact correlates to the initial thickness of the thin Ag film prior to the annealing step which determines the size distribution of the Ag nanoparticles (c.f. Fig. 2). A broad range of nanostructure distributions is apparent for the various types of back contacts. For Type I and Type V back contacts (deposited on the smallest and largest Ag NPs respectively), the maximum of the area-weighted base radius distribution is located around 30 nm and 530 nm, respectively. In first approximation, for all types of back contact, the height to radius aspect ratio of the nanostructures can be well approximated to be 0.75 (not shown).

In Fig. 4, measured diffuse reflectance spectra of the five types of Ag back contacts in air are shown. The diffuse reflectance increases from the Type I back contact to the Type V back contact with increasing average size of the nanostructures. Furthermore, the spectral range of enhanced diffuse reflectance shifts to longer wavelengths from the Type I back contact to the Type V back contact. For example, the maximum in diffuse reflectance is 45% at a wavelength of 586 nm for the back contact of Type II and 55% at a wavelength of 765 nm for the back contact of Type IV.

3.2. Optical simulation of reflectance spectra of Ag back contacts with non-ordered nanostructures

The measured diffuse and total reflectance spectra of the nanostructured back contacts in air shall be compared to simulated reflectance spectra. Due to the very high computational resources which are required for the simulation of nanostructured

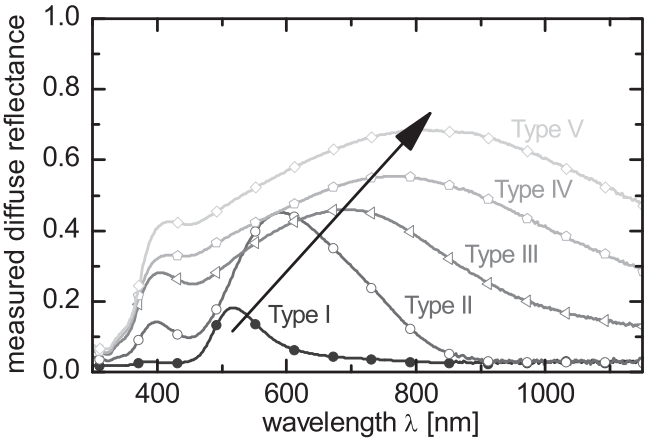

Fig. 4. Measured diffuse reflectance of five types of Ag back contacts with various distributions of non-ordered nanostructures.

Ag surfaces, it was not possible to simulate a representative surface area of the plasmonic Ag back contacts with non-regular nanostructures in a single simulation. Instead, the simulated reflectance spectra of these plasmonic Ag back contacts were calculated as an area weighted superposition of the simulated diffuse reflectance spectra of isolated nanostructures on Ag back contacts.

In a previous publication, LSP induced light scattering at isolated Ag nanostructures at back contacts of thin-film silicon solar cells was studied in detail with the simulation method used in this work [18]. In the present work, in order to represent the nanostructures of the five types of back contacts, optical simulations of isolated half-ellipsoidal nanostructures on Ag back contacts were performed. The base radius was varied in steps of 10 nm form 10 nm to 700 nm. This allows to cover the total range of detected base radii of the nanostructures of the five types of Ag back contacts (see Fig. 3). The height to base radius ratio was set to 0.75. A schematic cross-section of the structure is shown in the inset in Fig. 5. The simulated scattering efficiencies of the half ellipsoidal nanostructures in air are shown in Fig. 5. The scattering efficiency is derived a quotient of the power scattered by the nanostructure and the

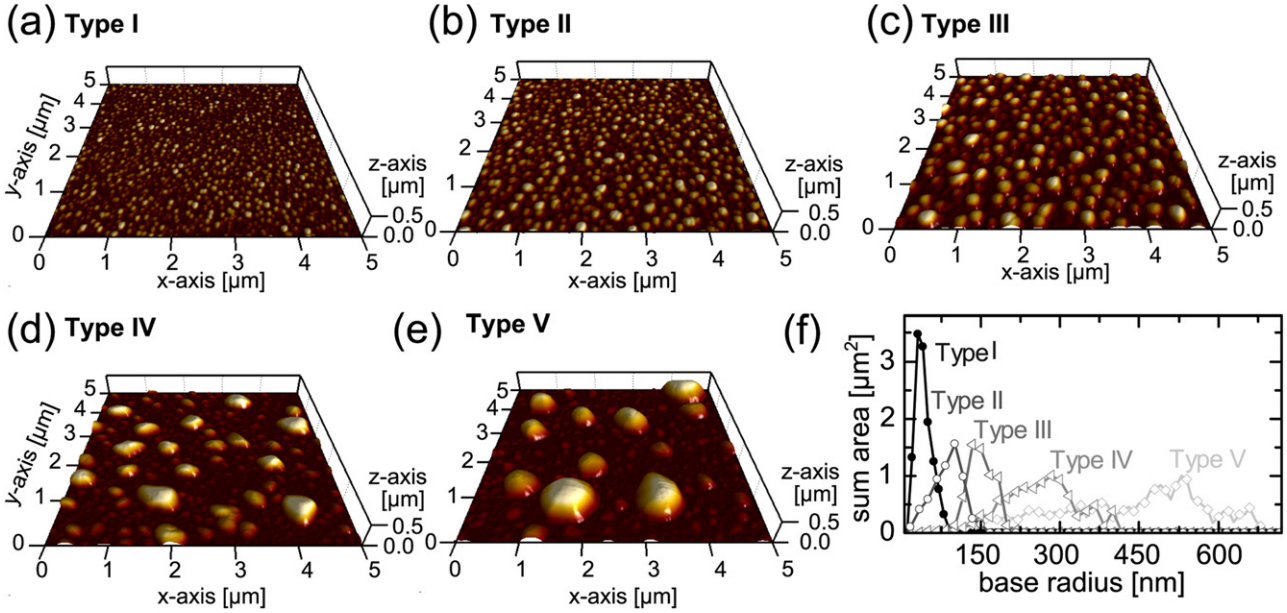

Fig. 3. (a)–(e) AFM images of five types of plasmonic back contacts with non-ordered Ag nanostructures. (f) Area-weighted base radius distribution (sum area) as a function of the base radius of the nanostructures derived from the AFM images.

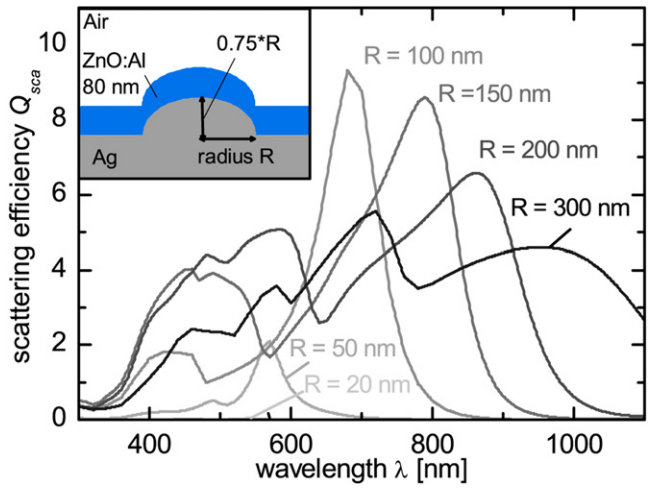

Fig. 5. Simulated scattering efficiency (Q_{sca}) of isolated ellipsoidal Ag nanostructures on Ag surfaces covered by a 80 nm thick ZnO:Al layer. The radius of the nanostructures is varied from 20 nm to 300 nm and the height is set to 75% of the corresponding radius.

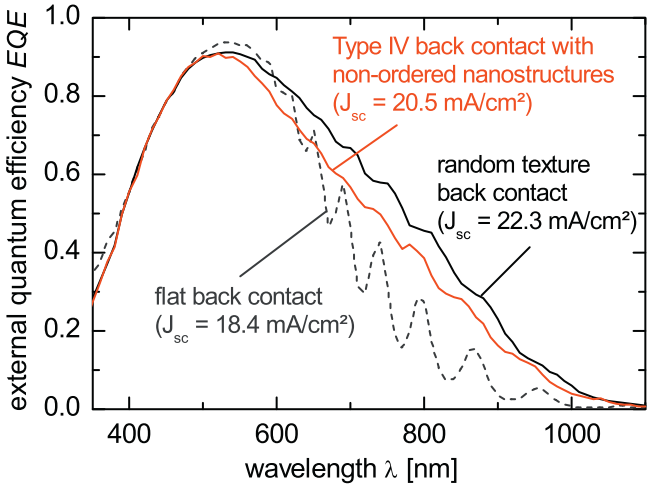

Fig. 7. External quantum efficiency of three μc-Si:H solar cells in n-i-p configuration codeposited on the flat back contact, the random texture back contact, and the Type IV back contact with non-ordered Ag nanostructures.

power irradiated on the cross section of the nanostructure. For LSP resonances, values of Q_{sca} above unity are possible. The harmonic oscillation of the electron gas in the nanostructure allows to enhance the optical cross section of the nanostructure beyond the geometrical cross section [9]. For small radii, only a dipolar LSP resonance is exhibited which shifts to longer wavelengths with increasing base radius of the nanostructures. The maximal in Q_{sca} increases for radii between 20 nm and 100 nm. For larger radii it decreases gradually and multipolar LSP resonances appear at shorter wavelengths. In addition, with increasing radius, the LSP resonances shift to longer wavelengths.

In order to derive the diffuse reflectance from the above presented simulations, the simulated spectra of Q_{sca} of the half-ellipsoidal nanostructures were weighted with the area-weighted base radius distribution of each type of plasmonic back contact. In Fig. 6, the resulting simulated diffuse reflectance of the five types of back contacts is shown. Two dominant trends are apparent. First, the diffuse reflectance increases gradually over the total wavelength range with increasing average base radius of the nanostructures on the back contacts. Second, the maxima in simulated diffuse reflectance shift to longer wavelengths with increasing base radius of the nanostructures of the back contacts. Both trends are apparent in the simulated diffuse reflectance spectra as well as

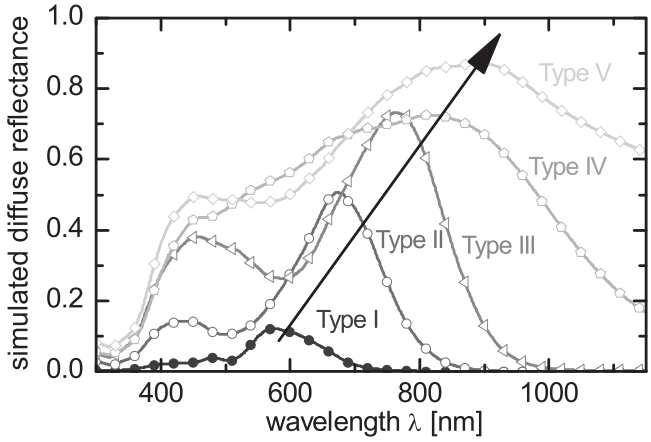

Fig. 6. Simulated diffuse reflectance of five types of Ag back contacts with various distributions of non-ordered nanostructures.

the measured reflectance spectra (c.f. Fig. 5). In fact, the overall characteristics of the measured diffuse reflectance spectra are well reproduced in the simulated spectra (aside of a factor). Thus, since the LSP resonances induce the scattering at the simulated Ag nanostructures, also the measured enhanced diffuse reflectance of the Ag back contact with non-ordered Ag nanostructures is attributed to an LSP-induced light scattering. The deviation in the total values of the measured and simulated diffuse reflectance as well as the redshift of the simulated spectra are attributed to the strong simplifications applied to derive the simulated diffuse reflectance spectra. Of particular importance are the simplified approximations of the nanostructures shape and size which are expected to account for these deviations. Also, the negligence of the electromagnetic coupling between adjacent nanostructures is expected to influence the spectral position of LSP resonances. However, in most cases, the coupling of two LSP modes in adjacent Ag nanoparticles causes a shift of the LSP resonance to longer wavelengths [9] which would induce an even larger spectral discrepancy of the maxima in the simulated and measured diffuse reflectance. Additional factors of influence on the spectral position of the LSPP resonances are the oxidation of the Ag nanostructures and the local variations in homogeneity of the ZnO:Al layer.

The above discussed diffuse reflectance of the back contacts in air confirmed the strong LSP-induced light scattering at the fabricated Ag back contacts with non-ordered nanostructures. It is expected that a comparable LSP-induced diffuse reflectance at these back contacts is apparent if they are incorporated into a thin-film silicon solar cell with a 80 nm thick ZnO:Al interlayer. However, with regard to the in-depth analysis of the light-trapping in thin-film silicon solar cells, the light scattering into the silicon absorber layer of the solar cells will be analyzed in future work.

3.3. Prototype solar cell

In Fig. 7, the measured EQE spectra of the three μc-Si:H solar cells in n-i-p substrate configuration codeposited on the flat back contact, the random texture back contact, and the Type IV Ag back contact with non-ordered nanostructures are shown. The Type IV back contact selected as it is the back contact with the second highest plasmon-induced light-scattering but exhibits nanostructures of height significantly smaller than the solar cell thickness (in contrast to type V). The Type IV back contact exhibits an average nanostructure base radius around 300 nm and a strongly enhanced diffuse reflectance (in air) for wavelengths longer than 500 nm (see

Fig. 4). For wavelengths above 520 nm the EQE of the solar cell deposited on the Type IV back contact is significantly enhanced in comparison to the EQE of the solar cell deposited on the flat back contact. The corresponding J_{sc} are enhanced from 18.4 mA/cm^2 to 20.5 mA/cm^2. This shows that the solar cell deposited on the plasmonic back contact exhibits a significantly improved light trapping. A substantial amount of incident light is guided inside the μc-Si:H absorber layer of the solar cell via light scattering at the back contact. In a recent work, the importance of light-scattering at the rear side of thin-film silicon solar cells in terms of light-trapping has been proven [4]. As demonstrated in the previous section, the light-trapping effect presented in this work can be correlated to LSP-induced light scattering at the Ag back contact with non-ordered nanostructures. Nevertheless, for the presented type of back contact the J_{sc} of the solar cell applying the plasmonic back contact remains 1.8 mA/cm^2 below the J_{sc} of the solar cell applying the conventional random texture light trapping. Thus, for the given nanostructure distributions at the Type D back contact, the light trapping is not competitive with the state-of-the-art texture for light trapping. In future work we will study the light scattering of the back contacts at the rear side of the solar cell into the silicon absorber layers of the solar cell. Based on future simulation-based optimizations of the shape, size as well as embedding layer stack of the Ag nanostructures, the additional improvement potential of the light-trapping effect will be researched.

4. Conclusion

In this contribution, we report on the preparation, characterization and optical simulation of plasmonic Ag back contacts with non-ordered Ag nanostructures. These back contacts are evaluated in terms of the light trapping in μc-Si:H thin-film silicon solar cells. The prepared Ag back contacts exhibit Ag nanostructures of base radius distribution maxima between 30 nm and 500 nm. Measured optical reflectance spectra of these Ag back contacts with non-ordered nanostructures in air are correlated to reflectance spectra calculated from three-dimensional electromagnetic simulations of localized surface plasmons in isolated nanostructures on Ag back contacts. Due to the very good agreement between the measured and simulated reflectance spectra of the various types of Ag back contacts with non-ordered nanostructures, it was possible to attribute the enhanced diffuse reflectance to plasmon-induced light scattering at the nanostructures of the back contacts. Importantly, this diffuse reflectance is exhibited by plasmon-induced light scattering at individual nanostructures, rather than collective effects such as diffraction as reported for plasmonic gratings [16–18].

The first prototype μc-Si:H n-i-p solar cell on one type of plasmonic Ag back contact with non-ordered half-ellipsoidal Ag nanostructures showed a significantly enhanced EQE for wavelengths longer than 500 nm when comparing to flat back contacts. The associated light-trapping effect is attributed to LSP-induced scattering at nanostructures on the back contact. However, when comparing to the solar cell applying a random texture back contacts, the EQE of the solar cell applying the Ag back contact with non-ordered is low. Further improvement are expected by simulation-based optimizations of the shape and size as well as embedding layer stack of the Ag nanostructures at the back contact, as well as optimization of silicon layers deposition on the nanostructured Ag back contacts.

Acknowledgements

The authors thank K. Bittkau, U. Aeberhard, W. Böttler, T. Merdzhanova, F. Finger, Aad Gordijn, G. von Plessen, D. Michaelis, C. Waechter and S. Burger for helpful discussions. The financial support from the German Federal Ministry of Education and Research under contract 03SF0354D is acknowledged.

References

[1] J. Meier, E. Vallat-Sauvain, S. Dubail, U. Kroll, J. Dubail, S. Golay, L. Feitknecht, P. Torres, S. Fay, D. Fischer, A. Shah, Solar Energy Materials and Solar Cells 66 (2001) 73–84.
[2] B. Rech, T. Repmann, M.N. van den Donker, M. Berginski, T. Kilper, J. Hüpkes, S. Calnan, H. Stiebig, S. Wieder, Thin Solid Films 511–512 (2006) 548–555.
[3] J. Müller, B. Rech, J. Springer, M. Vanecek, Solar Energy 77 (2004) 917–930.
[4] K. Bittkau, W. Böttler, M. Ermes, V. Smirnov, F. Finger, Journal of Applied Physics 111 (2012) 083101.
[5] H.A. Atwater, A. Polman, Nature Materials 9 (2010) 205–213.
[6] K.R. Catchpole, A. Polman, Optics Express 16 (2008) 21793–21800.
[7] F. Hallermann, C. Rockstuhl, S. Fahr, G. Seifert, S. Wackerow, H. Graener, G. von Plessen, F. Lederer, Physica Status Solidi (A) 205 (2008) 2844–2861.
[8] V.E. Ferry, J.N. Munday, H. Atwater, Advanced Materials 22 (2010) 4794–4808.
[9] U. Kreibig, M. Vollmer, Optical Properties of Metal Clusters, Springer-Verlag, Berlin, 1995.
[10] F.J. Beck, A. Polman, K.R. Catchpole, Journal of Applied Physics 105 (2009) 114310.
[11] K.R. Catchpole, A. Polman, Applied Physics Letters 93 (2008) 191113.
[12] E. Moulin, J. Sukmanowski, P. Luo, R. Carius, F. Royer, H. Stiebig, Journal of Non-Crystalline Solids 354 (2008) 2488–2491.
[13] E. Moulin, J. Sukmanowski, M. Schulte, A. Gordijn, F. Royer, H. Stiebig, Thin Solid Films 516 (2008) 6813–6817.
[14] C. Eminian, F.-J. Haug, O. Cubero, X. Niquille, C. Ballif, Progress in Photovoltaics: Research and Applications 19 (2011) 260–265.
[15] R. Santbergen, T.L. Temple, R. Liang, A.H.M. Smets, R.A.C.M.M. van Swaaij, M. Zeman, Journal of Optics 14 (2012) 024010.
[16] V.E. Ferry, M. Verschuuren, H.B.T. Li, E. Verhagen, R.J. Walters, R.E.I. Schropp, H.A. Atwater, A. Polman, Optics Express 18 (Suppl. 2) (2010) A237–A245.
[17] U.W. Paetzold, E. Moulin, D. Michaelis, W. Böttler, C. Wächter, V. Hagemann, M. Meier, R. Carius, U. Rau, Applied Physics Letters 99 (2011) 181105.
[18] U.W. Paetzold, E. Moulin, B.E. Pieters, R. Carius, U. Rau, Optics Express 19 (Suppl. 6) (2011) A1219–A1230.
[19] W. Böttler, V. Smirnov, A. Lambertz, J. Hüpkes, F. Finger, Physica Status Solidi 7 (2010) 1069–1072.
[20] SPIP v 5.1.6 – Particle and Poor Analysis, Image Metrology A/S, Denmark, 2011.
[21] "JCMsuite v2.4", retrieved from http://www.jcmwave.com JCMWave GmbH, Germany (2010).